Visual Perceptual Learning Enhances Functional Connectivity in Retinotopic Space

Vikranth R. Bejjanki[1] and Nicholas B. Turk-Browne[2]

Abstract

■ Repeated exposure to perceptual tasks improves behavioral performance. Several neural mechanisms have been proposed to account for such perceptual learning. Computational modeling suggests that plasticity in the connectivity between cortical sites may be responsible, by increasing the fidelity with which task-relevant information is transmitted through sensory hierarchies. Here, we explore this theory in humans using fMRI, testing the hypothesis that perceptual learning at one location in space will increase functional connectivity between voxels in visual areas that are tuned to that retinotopic location. Participants learned to detect one of two novel visual shape contours embedded in a noisy background in different visual quadrants. At baseline, there was no difference in behavioral sensitivity for the two shapes, nor a difference in functional connectivity between voxels in V1 and V4 responsive to the retinotopic locations of the two shapes. After training, there was a robust and selective improvement in perceptual detection of the trained shape relative to the control shape, along with increased functional connectivity between V1 and V4 voxels coding for the location of the trained shape in retinotopic space. Moreover, this increase in functional connectivity for the trained versus control shape predicted the improvement in behavioral sensitivity across participants. These results are consistent with the proposal that perceptual learning alters network dynamics so as to enhance the processing of behaviorally relevant information. ■

INTRODUCTION

Repeated exposure to perceptual tasks results in large improvements in performance (Lu & Dosher, 2022; Fahle, Edelman, & Poggio, 1995; Karni & Sagi, 1991; Fiorentini & Berardi, 1980). Such perceptual learning has been observed in a wide range of tasks and across modalities, suggesting that it represents a general mechanism by which humans and animals adapt their behavior to task demands (Seitz & Watanabe, 2005; Fine & Jacobs, 2002; Recanzone, Schreiner, & Merzenich, 1993; Recanzone, Jenkins, Hradek, & Merzenich, 1992; Gibson, 1963). Notably, perceptual learning tends to be specific to the features of the trained task (Gilbert, Sigman, & Crist, 2001; Ahissar & Hochstein, 1997; Crist, Kapadia, Westheimer, & Gilbert, 1997; Fahle & Morgan, 1996). For instance, behavioral improvements from training on orientation discrimination or shape identification at one location in space do not transfer to other locations or to other stimuli at the same location (Jia et al., 2020; Jehee, Ling, Swisher, van Bergen, & Tong, 2012; Lewis, Baldassarre, Committeri, Romani, & Corbetta, 2009; Schoups, Vogels, Qian, & Orban, 2001). Such specificity suggests an early locus of learning, where neural responses retain specificity to stimulus attributes (Watanabe et al., 2002). Indeed, previous neurophysiological (Yan et al., 2014; Adab & Vogels, 2011; Raiguel, Vogels, Mysore, & Orban, 2006; Yang & Maunsell, 2004; Schoups et al., 2001) and neuroimaging studies (Jia et al., 2020; Jehee et al., 2012; Bao, Yang, Rios, He, & Engel, 2010; Yotsumoto, Watanabe, & Sasaki, 2008; Kourtzi, Betts, Sarkheil, & Welchman, 2005; Furmanski, Schluppeck, & Engel, 2004; Schwartz, Maquet, & Frith, 2002; Ress, Backus, & Heeger, 2000) have documented changes in neural responses and BOLD activity in early visual areas as a result of perceptual learning.

The mechanism that mediates these changes is less clear. One early and prominent proposal is that perceptual learning is mediated through a steepening (i.e., amplification or sharpening) of neural tuning curves in early sensory areas via changes to lateral connections within these areas (Schwabe & Obermayer, 2005; Teich & Qian, 2003). This proposal is consistent with the observed changes in neural response properties in early visual areas like V1 and V4. However, neural responses are correlated in vivo (Ni, Ruff, Alberts, Symmonds, & Cohen, 2018; Smith & Kohn, 2008; Averbeck, Latham, & Pouget, 2006; Zohary, Shadlen, & Newsome, 1994), and it has been suggested that steepening of tuning curves need not lead to more informative neural representations or improved behavioral performance when noise correlations are considered (Kohn, Coen-Cagli, Kanitscheider, & Pouget, 2016; Seriès, Latham, & Pouget, 2004; Spiridon & Gerstner, 2001). Computational modeling instead suggests that plasticity in the connectivity between cortical areas may contribute

[1]Hamilton College, Clinton, NY, [2]Yale University, New Haven, CT

© 2026 Massachusetts Institute of Technology

Journal of Cognitive Neuroscience 38:9, pp. 1695–1707
https://doi.org/10.1162/JOCN.a.2620

Downloaded from direct.mit.edu/jocn/article-pdf/38/9/1695/2600227/jocn.a.2620.pdf by Yale University user on 13 October 2026

by increasing the fidelity with which task-relevant information is transmitted (Bejjanki, Beck, Lu, & Pouget, 2011). Specifically, changes in connectivity between early visual areas that better match the stimulus profile (i.e., by moving closer to a matched filter for the stimulus) can induce amplification and sharpening of tuning curves in early visual areas and result in highly specific behavioral improvements.

In the current study, we test this proposal noninvasively in humans at the level of fMRI. We employed a task in which participants detected shape stimuli defined by a closed contour of collinear Gabor elements embedded in a background of randomly oriented Gabors (Figure 1A). Two novel shapes (mirror reflections of each other) were presented in symmetric retinotopic locations in the top left and top right quadrants of visual field. We trained participants to detect one of the shapes (the "trained" shape) and measured perceptual sensitivity for this shape and the other "control" shape before and after training (Figure 1C). We evaluated the neural consequences of this training by defining visual areas V1 and V4 retinotopically in each participant and used population receptive field (pRF) mapping (Harvey & Dumoulin, 2011; Dumoulin & Wandell, 2008) to identify voxels in these areas coding for the precise retinotopic location of the trained and control shapes. This design does not allow us to directly test whether learning leads to neural changes such as amplification and sharpening of tuning curves. However, in line with the theoretical proposal that inspired this study, we hypothesized that, from before to after training, participants would show increased perceptual sensitivity and greater retinotopically specific functional connectivity for the trained versus control shape, and that these behavioral and neural changes would be associated across participants.

METHODS

Participants

Twenty-four naive adults (nine men; ages 18–31 years, mean = 22.8 years) with normal or corrected-to-normal visual acuity from the Princeton University community participated in two fMRI sessions for monetary compensation ($20/hr). Four additional participants were excluded due to an inability to complete a scanning session or because they did not return for the second scanning session. This sample size is similar to or exceeds that used in prior fMRI studies examining perceptual learning in humans (e.g., Jia et al., 2020; Jehee et al., 2012; Lewis et al., 2009; Kourtzi et al., 2005). The Princeton University institutional review board approved the study protocol, and all participants provided informed consent.

Stimuli

The stimuli were inspired by prior studies (Kourtzi et al., 2005). Two novel shapes (Figure 1A) were rendered with collinear Gabor elements (0.4°) and embedded in

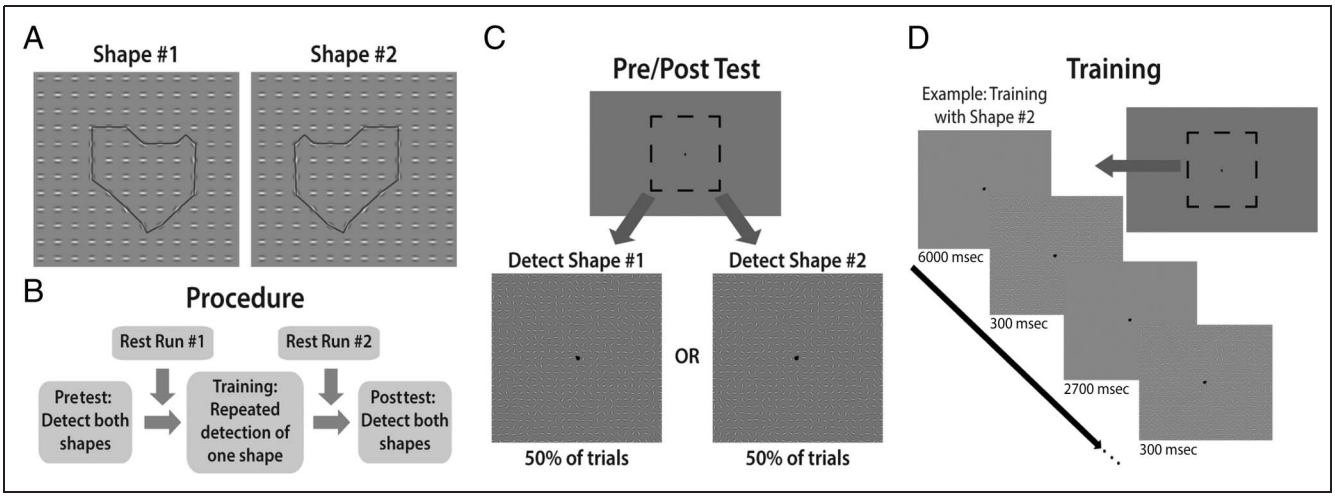


Figure 1. Experimental paradigm. (A) Shapes. Two novel shapes were rendered with collinear Gabor elements and embedded in backgrounds of randomly oriented Gabors (horizontal background Gabors and black shape outline shown only for illustrative purposes). The two shapes were mirror reflections of each other and were presented at symmetric retinotopic locations to the top left and top right quadrants of fixation. (B) Procedure. Participants were trained to detect one "trained" shape, with sensitivity for this shape and the "control" shape assessed before and after training. Six runs of fMRI data were collected while participants completed the training task. Rest runs were collected immediately before and after training to assay changes in functional connectivity, during which participants fixated a central fixation symbol. (C) Pre/post shape detection task. After the presentation of a fixation symbol (a teardrop symbol), participants were cued to report the presence or absence of one of the shapes (signaled by the teardrop pointing to the top left or top right quadrant) while maintaining central fixation. The dashed black box illustrates the central stimulus area spanning the Gabor display (including the shape and background elements—enlarged below for descriptive purposes). No performance feedback was provided. (D) Training task. An illustration of the start of a training block for an example participant. In each block of training, after an initial fixation period, participants were repeatedly cued to report the presence or absence of the trained shape for that participant (shape #2 in this example). The dashed black box illustrates the central stimulus area spanning the Gabor display (including the shape and background elements—enlarged for descriptive purposes). Accuracy feedback was provided at the end of each training block.

Downloaded from direct.mit.edu/jocn/article-pdf/38/9/1695/2600227/jocn.a.2620.pdf by Yale University user on 13 October 2026

backgrounds (25 × 25 grid) of randomly oriented Gabors. Each shape involved a closed contour of 18 collinear Gabor elements (average shape area: 4.9° × 4.9°). The two shapes were mirror reflections across the vertical meridian and were presented at symmetric retinotopic locations to the left and right of fixation in the upper visual field (Figure 1C). The starting orientations of the background Gabor elements were drawn from a uniform distribution centered on 90° (training task: range = [38, 142], pre/post task: range = [30, 150]), and the starting separation (center-to-center) of individual Gabor elements was 0.75°. To ensure that participants learned the shapes and not the background configuration, the orientation and position of each Gabor element was randomly jittered on every trial, with the jitter level set to make the shape detection task challenging (based on results from pilot tests). The display also included a teardrop-shaped fixation point (0.4°), located at the center of the display (replacing the Gabor element at that location).

Procedure

Each participant completed two experimental sessions, separated by 0–2 days. During the first session, participants completed two variants of the shape detection task: (1) a training task, in which they were trained to detect one of the novel shapes; and (2) a pre/post task, in which their sensitivity to detecting both shapes was assessed before and after training. Six fMRI runs were collected while participants completed the training task, preceded and followed by a rest run (Figure 1B). The second experimental session was used to collect structural images and six additional fMRI runs for retinotopic mapping.

Pre/Post Task

During the first experimental session, participants performed the shape detection task in the MRI scanner. Stimuli were projected on a screen behind the scanner and viewed with a mirror on the head coil. Participants first performed a pretest (Figure 1C) to assess their baseline sensitivity for detecting the two shapes. They were told that they would be presented with several trials in which they would see a grid of small oriented objects, with a black teardrop-shaped symbol in the middle. They were instructed to keep their eyes fixated on this central fixation point at all times in the experiment and were told that this was important for the goals of the study. On each pretest trial, the teardrop pointed to either the top left or to the top right quadrant of the display for 300 msec, after which the Gabor grid was presented for 300 msec. The display then reverted to showing a centrally oriented teardrop symbol, and participants were tasked with reporting whether or not they had detected a shape in the cued quadrant while maintaining central fixation. No time limit was imposed on their response. For instance, if the fixation symbol pointed to the top left on a particular trial, participants performed a two-alternative forced-choice task on whether they detected the shape in the top left quadrant. When there was a shape present, it was always the same shape in the top left quadrant, while the other shape was always in the top right quadrant. Participants completed a total of 80 trials during the pretest, with 40 trials cuing the top left quadrant and 40 trials cuing the top right quadrant (randomly intermixed). The cued shape was present in 50% of the trials (see Reppa, Williams, Greville, & Saunders, 2020; Aly & Turk-Browne, 2016; Fisher & Sloutsky, 2005, for prior studies using a similar number of trials to estimate behavioral sensitivity via A'). No performance feedback was provided to participants. Trials were separated by an intertrial interval of 1 sec. Participants did not undergo any familiarization trials prior to the pretest. While this might have resulted in some initial task learning or a practice effect that could affect the baseline measurement of perceptual sensitivity, this would be true for both trained and control shapes and would not explain any differences between shapes. At the conclusion of training, participants performed a posttest identical to the pretest.

Training Task

One shape was designated as the "trained" shape, and the other served as the "control" shape (counterbalanced across participants). The training task was almost identical to the pre- and posttests, except that it contained only the trained shape in its same location. Thus, the teardrop always pointed to either the top left or the top right quadrant, depending on the participant, and the procedure no longer included the initial 300-msec cue period used in the pre/posttests to signal the quadrant where the shape could appear. We collected six runs of fMRI data while participants performed the training task. Each run began with 6 sec of central fixation, followed by 154 trials that began every 3 sec (total of 924 training trials). This timing included the stimulus display (Gabor grid with shape present on half of trials) being presented for 300 msec, followed by a fixation interval of 2700 msec. The run ended with 4 sec of fixation, for a total duration of 7 min 52 sec. Participants were instructed to keep their eyes fixated on the central fixation point (i.e., the teardrop symbol) throughout the run. Participants were provided feedback on their accuracy (as percent correct) at the end of each run. During the first three training runs, the presence/absence of the trained shape was randomly ordered across trials. The order for the last three runs was mirrored with the first three runs, such that Runs 1 and 6, Runs 2 and 5, and Runs 3 and 4 involved identical presentation orders.

Rest Runs

We also collected fMRI data during two rest runs, each of which was the same duration as the training runs (7 min 52 sec). During the rest runs, only the fixation point was

Downloaded from direct.mit.edu/jocn/article-pdf/38/9/1695/2600227/jocn.a.2620.pdf by Yale University user on 13 October 2026

presented on the screen, and participants were instructed to keep their eyes open and stare at the fixation. The first rest run was collected after the pretest but before the start of training, whereas the second rest run was collected after the last training run but before the start of the posttest (Figure 1B). Eye position was monitored at 60 Hz with an iViewX MRI-LR eye tracker (SMI). Because of technical difficulties, eye-tracking data could not be collected from three participants.

Retinotopic Mapping

We performed phase-encoded retinotopic mapping during the second experimental session using standard procedures (Al-Aidroos, Said, & Turk-Browne, 2012; Arcaro, McMains, Singer, & Kastner, 2009). A flickering and colorful circular checkerboard (4 Hz flicker, 14° radius) was shown at fixation to stimulate visual receptive fields. During polar angle runs, which were used to map the preferred polar angle of voxels, the checkerboard was masked so that only a 45° wedge was visible, and the mask rotated clockwise or counterclockwise at a rate of 9°/sec creating the perception of a rotating wedge with a 40-sec period. During eccentricity runs, which were used to map the preferred eccentricity of voxels, the checkerboard was masked to create the perception of an expanding or contracting annulus. The expansion/contraction period was 40 sec, and the thickness and rate of expansion of the annulus increased logarithmically with eccentricity to approximate the cortical magnification factor of early visual cortex. Participants completed six total retinotopic mapping runs (order counterbalanced across participants): one run each in which the checkerboard wedge rotated clockwise or counterclockwise, one run each in which the checkerboard ring expanded or contracted, and then another run each in which the checkerboard rotated clockwise or counterclockwise. All runs had the same duration (5 min 52 sec). To ensure that participants were actively attending to the stimuli, they were instructed to detect when a central fixation point (radius = 0.25°) dimmed from white to gray (every 2–5 sec) using a button box.

Data Analysis

Acquisition

Tasks were conducted with the Psychophysics Toolbox (https://psychtoolbox.org) for MATLAB (MathWorks, Inc.). fMRI data were acquired at the Scully Center for the Neuroscience of Mind and Behavior at Princeton University with a 3T Siemens Skyra MRI scanner using a 16-channel head coil.

Functional images for the training and rest runs were acquired using a gradient-echo EPI sequence (repetition time [TR] = 500 msec, echo time [TE] = 30 msec, flip angle [FA] = 60°, matrix = 64 × 64, resolution = 3 × 3 × 3 mm, multiband acceleration factor = 3) with 21 interleaved oblique slices (15° transverse to coronal). A short TR was used to prioritize collecting as many time points as possible for functional connectivity analyses. These parameters resulted in a partial brain volume for each participant; we positioned the slice slab over the occipital and temporal lobes to maximize spatial and temporal resolution over our a priori visual ROIs. Stimulus onsets were time-locked to the start of TRs. Functional images for retinotopic mapping runs were acquired with a gradient-echo EPI sequence (TR = 2 sec, TE = 40 msec, FA = 71°, matrix = 128 × 128, resolution = 2 × 2 × 2.5 mm) with 25 interleaved slices aligned to the calcarine sulcus.

For each scanning session and functional sequence, we also collected a T1 FLASH anatomical scan, co-planar to the functional scans, to improve registration. To correct for B0-field inhomogeneity, phase and magnitude field maps were collected toward the end of each session (i.e., after all functional scans), co-planar with the functional scans and with the same resolution. Finally, a high-resolution (0.9 × 0.9 × 0.9 mm) T1 MPRAGE anatomical scan was acquired at the end of the second session for surface reconstruction and registration.

Preprocessing

fMRI data were analyzed using the FMRIB software library (FSL) (Smith et al., 2004), FreeSurfer (Dale, Fischl, & Sereno, 1999), AFNI (Cox, 1996), SUMA (https://afni.nimh.nih.gov/afni/suma/), and MATLAB. All images were skull-stripped to improve registration. Volumes from the first 6 sec of functional runs were discarded. The remaining volumes were corrected for slice-acquisition time and head motion, high-pass filtered (retinotopic mapping runs: 100-sec cutoff; training and rest runs: 128-sec cutoff), spatially smoothed (retinotopic mapping runs: 3-mm FWHM; training and rest runs: 5-mm FWHM), and registered to the FLASH, MPRAGE, and Montreal Neurological Institute standard brain.

ROIs

Based on the retinotopy runs, we manually drew occipital ROIs for V1–V4 in both hemispheres using Freesurfer, AFNI, and SUMA following previously published procedures (Arcaro et al., 2009). To visualize occipital areas simultaneously, each participant's cortical surface was segmented along the white matter/gray matter boundary and then inflated and flattened. Functional runs from retinotopic mapping sessions were pre-whitened, corrected for hemodynamic lag (3 sec), and phase-decoded to determine the angle and eccentricity of maximal stimulation for each voxel in visual cortex. We further accounted for hemodynamic lag by averaging phase estimates from clockwise/counterclockwise and expansion/contraction runs. We projected the decoded phase values onto the cortical surface and determined occipital ROIs according to the relative locations of polar-angle reversals and

Downloaded from direct.mit.edu/jocn/article-pdf/38/9/1695/2600227/jocn.a.2620.pdf by Yale University user on 13 October 2026

foveally stimulated regions (Arcaro et al., 2009; Wandell, Dumoulin, & Brewer, 2007).

Resting Connectivity

To infer functional connectivity between voxels in V1 and V4, we computed temporal correlations between their BOLD time series during the rest runs. Such correlations have been used extensively in the literature to infer the latent functional architecture at rest (Fox & Raichle, 2007; Biswal, Yetkin, Haughton, & Hyde, 1995). After preprocessing, BOLD signal from the rest runs was scrubbed of nuisance variance using a general linear model, which contained regressors for the global mean activity, six motion correction parameters obtained from preprocessing, and the activity from two (posterior) white matter voxels and two (posterior) ventricle voxels. We inferred the resting connectivity between pairs of voxels by computing the temporal Pearson correlation over the residuals from this model.

Because we expected learning to influence functional connectivity in a spatially specific manner, we also estimated pRFs. This provided a continuous estimate of the visual field location(s) to which each voxel responded. For each ROI, we used the phase-decoded angle and eccentricity of maximal stimulation for each voxel (computed from retinotopic mapping runs) to estimate the visual field location of maximal response (Engel, Glover, & Wandell, 1997). We then combined this information—the center location (x, y) for the pRF—with published estimates of pRF size (σ) as a function of area and eccentricity (Harvey & Dumoulin, 2011) to derive an isotropic two-dimensional Gaussian pRF model of visual field locations per voxel.

We combined these estimates to compute functional connectivity between voxels in V1 and V4. We hypothesized that learning to detect a shape at one location in visual space would enhance functional connectivity between voxels in V1 and V4 that respond to that location. To test this hypothesis, we computed a weighted average of the resting connectivity between each V4 voxel in the trained and control quadrants, and all V1 voxels whose pRFs (1) were encompassed by the pRF of the V4 voxel and (2) overlapped the trained or control shape contour. The trained/control shape contours were defined as bands spanning a width approximately equal to the average center-to-center distance between Gabors in the grid (0.75°), centered on the locations of the Gabor elements defining each shape. A V1 voxel was included if at least 30% of its pRF overlapped the shape contour. This threshold was empirically chosen to maximize the overlap between V1 pRFs and the shape contour while ensuring that we had enough V1 voxels that could be included in our analysis (by this criterion) for each quadrant and participant. For each V4 voxel, we calculated a weighted average of functional connectivity across all included V1 voxels, with the weight determined by a Gaussian function of the distance between the V4 pRF center and the V1 pRF center. We then averaged this measure across all V4 voxels in each quadrant and repeated this process for the two rest runs to compute estimates of functional connectivity between voxels in V1 and V4 coding for the trained and control shapes for each participant and run.

In addition to this quadrant-averaged measure, we also sought to visualize the spatial pattern of functional connectivity before and after training. We projected the weighted average functional connectivity computed for each V4 voxel (using the above approach) back on to stimulus space, as a two-dimensional isotropic Gaussian density function, and generated an average value at each pixel in the stimulus display. Exploiting the fact that the control and trained shapes were mirror reflections of each other presented at symmetric retinotopic locations in their respective quadrants, we computed a normalized difference of the functional connectivity between V1/V4 voxels coding for the trained versus control shape in stimulus space. Specifically, for matching polar coordinates from fixation in both quadrants, we computed the normalized difference as $[FC_{Trained} - FC_{Control} / FC_{Trained} + FC_{Control}]$. Because it is possible to obtain negative values for functional connectivity and prior work has shown that the presence of negative values can bias such a metric, we computed this normalized difference after shifting all values by a constant to bring the most negative value to zero (Simmons, Bellgowan, & Martin, 2007).

Background Connectivity

To assess functional connectivity between V1 and V4 voxels during the training runs, we measured background connectivity. In the presence of external stimulation, as was the case during the training runs, the BOLD activity in different neural areas is correlated not only due to the connectivity between them but also due to the synchronized stimulus-evoked responses. By exploiting the fact that evoked (stimulus-driven) and spontaneous (connectivity-driven) correlations are linearly superimposed in human fMRI data (Fox, Snyder, Zacks, & Raichle, 2006), the background connectivity approach to inferring functional connectivity models and linearly regresses stimulus-evoked responses out of the data before measuring correlations in the residual spontaneous fluctuations (Tompary, Al-Aidroos, & Turk-Browne, 2018; Griffis, Elkhetali, Burge, Chen, & Visscher, 2015; Al-Aidroos et al., 2012; Norman-Haignere, McCarthy, Chun, & Turk-Browne, 2012).

After preprocessing, BOLD signal from the training runs was scrubbed of nuisance and stimulus-evoked variance using two general linear models. The first (nuisance) model contained regressors for the global mean activity, six motion correction parameters from preprocessing, and the activity from two (posterior) white matter voxels and two (posterior) ventricle voxels. Residuals from the nuisance model were the input to the second (evoked)

Downloaded from direct.mit.edu/jocn/article-pdf/38/9/1695/2600227/jocn.a.2620.pdf by Yale University user on 13 October 2026

model. As described earlier, each training run consisted of 154 trials, with the trained shape present in half the trials and absent in the other half. To capture the average evoked response when the shape was present/absent, we created two sets of 30 finite impulse response (FIR) regressors (one set for the shape present event and one set for the shape absent event). Each regressor had a delta function at the corresponding TR (500 msec) following the relevant event and zeros elsewhere, resulting in a data-driven estimate of the shape and timing of the evoked hemodynamic response function (HRF) over a window of 15 sec. The residuals of the FIR model, with the custom HRF removed, were correlated across V1 and V4 voxels, as described above for the rest runs, to assess background connectivity during the training runs.

Statistics

We used a nonparametric measure A' (Donaldson, 1992; Snodgrass & Corwin, 1988) to index behavioral sensitivity, as it is robust to the low hit rates we expected to obtain (particularly at the outset of the study). A' was calculated as follows (where H represents the hit rate and F represents the false alarm rate; Snodgrass & Corwin, 1988):

$$A' = \begin{cases} 0.5 + \dfrac{(H - F)(1 + H - F)}{4H(1 - F)} & \text{when } H \geq F \\ 0.5 - \dfrac{(F - H)(1 + F - H)}{4F(1 - H)} & \text{when } F > H \end{cases}$$

We used nonparametric bootstrap resampling (Efron & Tibshirani, 1986) to assess reliability for comparisons involving functional connectivity (r) values after variance stabilization using Fisher's r-to-z transformation; reported connectivity values are presented in the original r form to facilitate interpretation and visualization. We used the robust correlation toolbox (Pernet, Wilcox, & Rousselet, 2013) to calculate the brain–behavior relationship across participants between the normalized difference in connectivity of voxels coding for the trained versus control shape (formula above) and the normalized difference in behavioral sensitivity for the trained versus control shape $[A'_{\text{Trained}} - A'_{\text{Control}} / A'_{\text{Trained}} + A'_{\text{Control}}]$. Specifically, we used the robust skipped correlation method (accounting for bivariate outliers) to estimate the true coefficient of association (with accurate false positive control and without loss of power) and bootstrapped 95% confidence intervals to evaluate reliability. Finally, we used Steiger's Z test (Lee & Preacher, 2013; Steiger, 1980) to evaluate whether the two correlation coefficients obtained in this manner were reliably different from each other.

RESULTS

Behavior

Sensitivity for detecting the target shape improved substantially across the six runs of training (repeated-measures ANOVA: $F(5, 115) = 5.8$, $p = .00008$; Figure 2A). Of the 24 participants, 20 showed numerically better performance in the last versus first training run (Figure 2B). Comparing performance from before to after training revealed improved sensitivity for both the trained shape, $t(23) = 5.88$, $p = .000005$, and the control shape, $t(23) = 4.04$, $p = .0005$, suggesting a general benefit from practicing the detection task. Critically, however, the improvement in sensitivity was greater for the trained shape than the control shape, $t(23) = 2.56$, $p = .017$ (Figure 2C), consistent with specific perceptual learning of the trained shape in its quadrant.

Eye Tracking

Because the trained and control shape contours were presented in the top left and top right quadrants of fixation, gaze position was monitored during the pre- and post-training rest runs to ensure that there were no systematic biases toward either quadrant. Participants reliably maintained central fixation (average horizontal displacement of gaze position from fixation did not differ from zero) during both the pretraining, $t(20) = 1.63$, $p = .12$, and post-training, $t(20) = 0.53$, $p = .6$, rest runs. More specifically, we confirmed that participants did not reliably differ in the extent to which their mean gaze position was deployed to the trained versus control quadrants in each run (pretraining: $t(20) = 0.97$, $p = .34$; posttraining: $t(20) = 2.0$, $p = .06$) and that there was no significant difference between the two runs in participants' average horizontal gaze position, $t(20) = 0.53$, $p = .6$. Finally, we quantified the number of fixations (if any) that participants exhibited to the locations in which the trained or control shapes appeared. We found that the number of fixations to either shape location did not reliably differ from zero during both the pretraining (control: $t(20) = 1.27$, $p = .22$; trained: $t(20) = 1.03$, $p = .32$) and posttraining (control: $t(20) = 1.72$, $p = .1$; trained: $t(20) = 1.04$, $p = .31$) rest runs.

Resting Connectivity

What are the neural mechanisms that underlie the specific improvement we observed in shape detection performance? Here, we sought to test the theoretical proposal (Bejjanki et al., 2011) that changes in connectivity between visual areas may be responsible by increasing the fidelity with which task-relevant information is transmitted. Specifically, we expected Gabor elements in the stimulus display to stimulate responses in the primary visual cortex, which is known to encode basic stimulus features such as orientation and spatial frequency (Nauhaus, Nielsen, Disney, & Callaway, 2012; Ferster & Miller, 2000; Hubel & Wiesel, 1968) and to respond robustly to Gabor-like stimuli. Furthermore, we expected the representation of the target shape to arise further downstream in V4, which receives input from the primary visual cortex, has large receptive fields (thereby integrating input information

Downloaded from direct.mit.edu/jocn/article-pdf/38/9/1695/2600227/jocn.a.2620.pdf by Yale University user on 13 October 2026

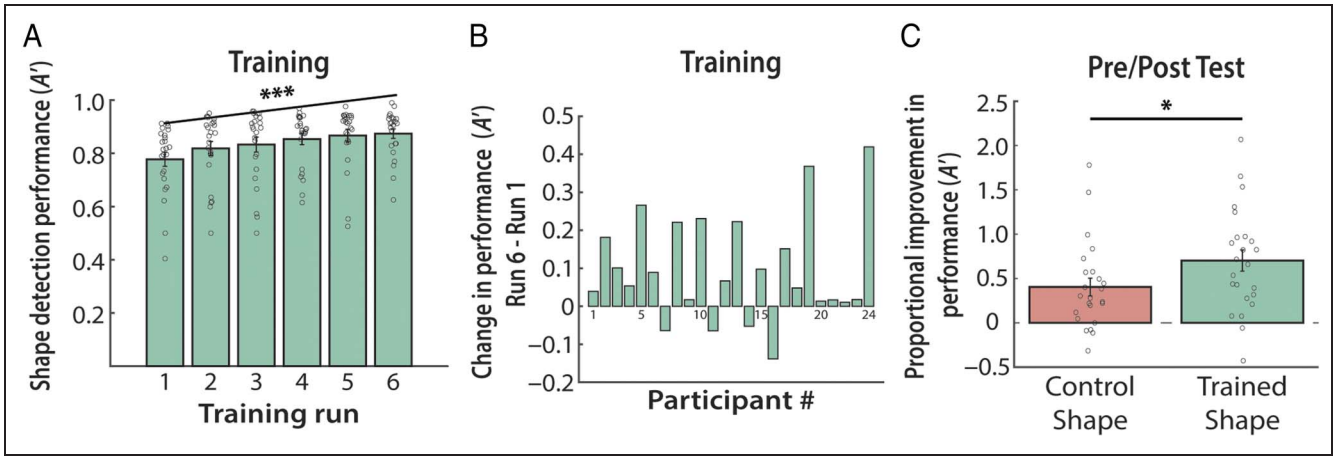


Figure 2. Shape detection performance, as indexed by a nonparametric measure of sensitivity (A'). (A) Participants improved in detecting the trained shape against a noisy background, as a function of training. (B) Most participants (20 of 24) demonstrated numerically better sensitivity for detecting the trained shape at the end of training (Run 6) than at the start (Run 1). (C) Participants showed improved posttraining performance, as a proportion of their pretraining performance, for both the control and trained shapes, but significantly more so for the trained shape. Dots indicate individual participants, bars represent the mean across participants, and error bars represent *SEM*. $*p < .05$, $***p < .001$.

pertaining to multiple Gabor elements), and is known to encode shape and object information (Thielscher, Kölle, Neumann, Spitzer, & Grön, 2008; Kastner, De Weerd, & Ungerleider, 2000). Thus, we expected the stimulus displays used in our task to be represented by retinotopically organized voxels in visual areas V1 and V4 (Riesenhuber & Poggio, 2000; Wallis & Rolls, 1997). We hypothesized that perceptual learning of a shape at one location in visual space would strengthen the coupling between voxels in V1 and V4 with overlapping pRFs tuned to that location.

To test this hypothesis, we compared V1–V4 functional connectivity during the pre- and posttraining rest runs in the visual field quadrants where the trained and control shapes appeared (Figure 3A). Because the rest runs occurred immediately before and after training, these runs provided a clean measure of how baseline functional connectivity was altered by perceptual learning. In the pretraining rest run, we did not observe a baseline difference in functional connectivity between V1 and V4 voxels coding for the quadrant of the trained versus control shape (bootstrap $p = .35$). However, in the posttraining rest run, this difference was marginally significant ($p = .06$); the interaction of run by condition was not significant ($p = .11$).

This analysis included V1 and V4 voxels whose preferred retinotopic locations were anywhere in the trained and control quadrants, which may have diluted effects that were retinotopically specific to the precise location of the trained shape contour. We therefore examined the spatial distribution of differences in functional connectivity by projecting the functional connectivity of each V4 voxel (weighted average of connectivity with overlapping V1 voxels) onto stimulus space and averaging across values

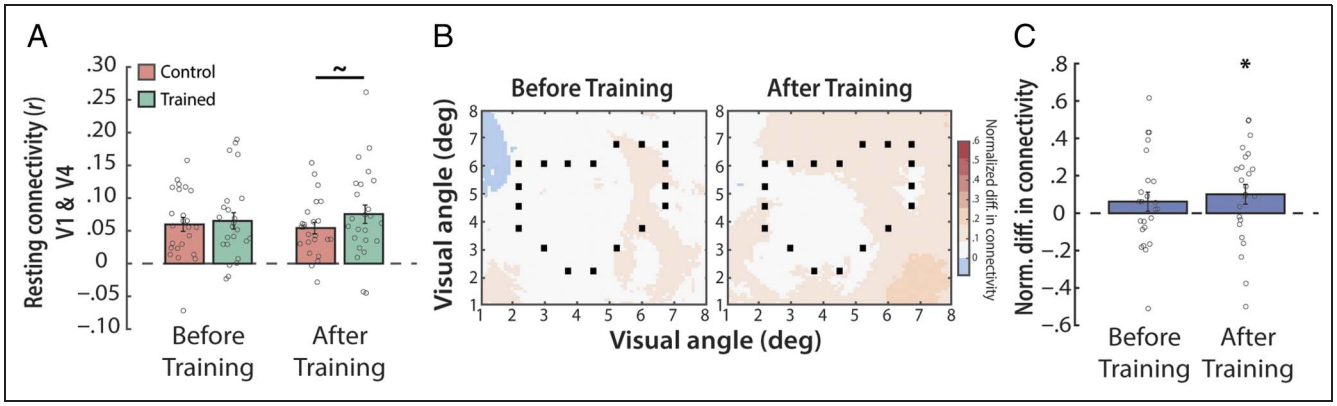


Figure 3. Resting functional connectivity before and after training. (A) Weighted average of the resting connectivity between voxels in V1 and V4 coding for the quadrant of the trained (green) and control (pink) shapes. Dots indicate individual participants, bars represent the mean across participants, and error bars represent *SEM*. (B) Group visualization in stimulus space of the difference in resting connectivity between V1 and V4 voxels coding for the locations of the trained versus control shape. The normalized difference in V1–V4 connectivity, averaged across participants, is shown for each cell in a 7°×7° grid centered on the shape contour. The locations of the individual Gabor elements that made up the shape contour are depicted with black squares. (C) Normalized difference in functional connectivity, specific to the shape contour, before and after training. $\sim p = .06$, $*p < .05$.

Downloaded from direct.mit.edu/jocn/article-pdf/38/9/1695/2600227/jocn.a.2620.pdf by Yale University user on 13 October 2026

at each pixel (Figure 3B). To quantify contour-specific changes in functional connectivity, we computed a normalized difference in functional connectivity along the contour of the trained versus control shape in the pre- and posttraining rest runs (Figure 3C). Consistent with the quadrant-level results, there was no reliable difference in the pretraining run ($p = .11$), but importantly, the effect in the posttraining run was clearer when restricted to the shape contour ($p = .03$); the interaction was not reliable ($p = .17$). Moreover, a control analysis, in which we similarly considered the normalized difference in functional connectivity in a "background" region that did not overlap with the shape contour, revealed no reliable differences in either the pretraining ($p = .27$) or posttraining ($p = .21$) runs, nor an interaction ($p = .5$).

Brain–Behavior Relationship

These results are based on averaging across all participants. However, there was considerable variability in behavioral perceptual learning (Figure 2B). We would not expect, for example, the four participants who did not improve behaviorally during training to exhibit greater functional connectivity for the trained shape from pre- to posttraining. Indeed, when we restricted the analysis shown in Figure 3A to the 20 participants who had numerically greater behavioral sensitivity in the last versus first training run (Figure 4A), the posttraining difference in V1–V4 functional connectivity between trained versus control quadrants changed from marginal to significant ($p = .009$) despite the smaller sample size; the run by condition interaction was marginal ($p = .05$). As expected, there was still no pretraining difference ($p = .29$).

This binary approach to identifying learners versus nonlearners obscures continuous variance across individuals. We thus performed a quantitative analysis of the relationship between learning-induced changes (normalized difference of trained vs. control shapes) in behavioral sensitivity and resting functional connectivity across the full sample (Figure 4B). Indeed, there was a significant positive brain–behavior correlation after training ($r_{skipped} = .55$, bootstrapped 95% CI [.12, .75]). This was not a generic effect of individual differences, as the relationship was not reliable before training ($r_{skipped} = -.02$, bootstrapped 95% CI [−.39, .40]). Notably, the correlation after training was reliably different from the correlation before training (Steiger's Z test: $p = .037$). Thus, for a given participant, the extent to which functional connectivity between V1 and V4 voxels coding for the trained (vs. control) shape increased with training predicted the extent to which behavioral sensitivity increased.

Functional Connectivity during Training

We included rest runs immediately before and after training to obtain a clean primary measure of learning-induced changes in functional connectivity between visual areas unconfounded by stimulus responses and task demands. For completeness, we also explored a secondary measure of changes in functional connectivity during training. Namely, we calculated background connectivity between voxels in V1 and V4 by first regressing out noise sources and stimulus-evoked responses and then computing correlations in the residual BOLD time series. Although the background connectivity between V1 and V4 voxels coding for the quadrant of the trained shape was numerically greater than that between voxels coding for the quadrant of the control shape, these differences were not reliable (all ps > 0.1; Figure 5A).

Despite the lack of an overall effect, we next explored whether background connectivity was behaviorally relevant. For each training run, we correlated the trained versus control difference in V1–V4 background connectivity with the difference in behavioral sensitivity for the trained versus control shape after training. During the first training run, there was no relationship between background connectivity and posttraining behavioral sensitivity ($r_{skipped} = .36$,

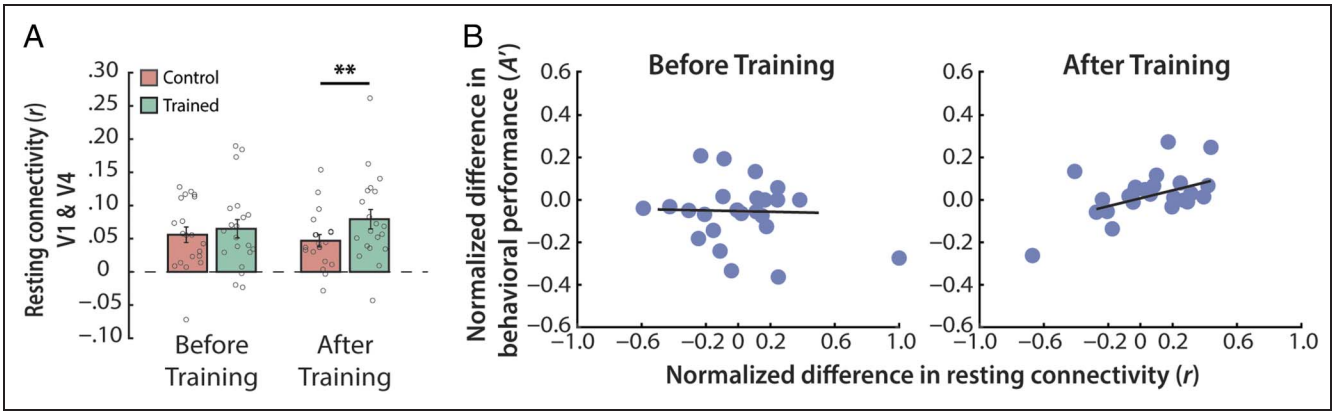


Figure 4. Brain–behavior relationships. (A) Functional connectivity, before and after training, for the 20 (of 24) participants who showed improved behavioral performance in the last versus first training run. Dots indicate individual participants, bars represent the mean across participants, and error bars represent *SEM*. (B) Robust correlations between the normalized difference in resting functional connectivity for voxels coding for the quadrant of the trained versus control shape and the normalized difference in behavioral sensitivity for detecting the trained versus control shape. Dots represent individual participants.

Downloaded from direct.mit.edu/jocn/article-pdf/38/9/1695/2600227/jocn.a.2620.pdf by Yale University user on 13 October 2026

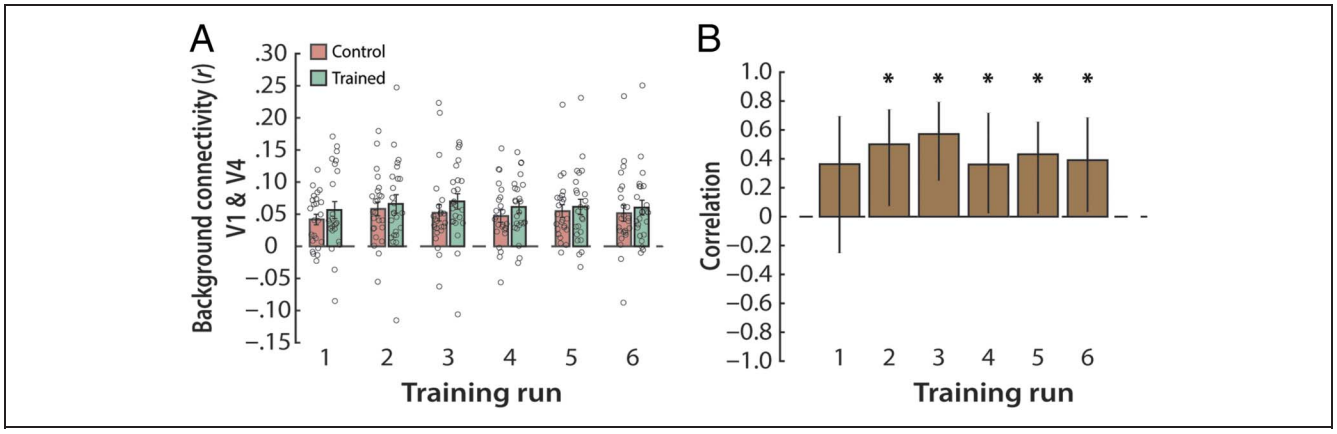


Figure 5. Functional connectivity during training. (A) Weighted average of the background connectivity between voxels in V1 and V4 coding for the quadrant of the trained (green) and control (pink) shapes. Dots indicate individual participants, bars represent the mean across participants, and error bars represent *SEM*. (B) Robust correlations between the normalized difference in background connectivity for voxels coding for the quadrant of the trained versus control shape and the normalized difference in posttraining behavioral sensitivity for the trained versus control shape. Bars represent best-fit correlation coefficients and error bars represent 95% bootstrapped confidence intervals, obtained using the robust skipped correlation method. *$p < .05$.

bootstrapped 95% CI [−.25, .69]). However, during each of the remaining five runs, the relationship was positive and reliable (Run 2: $r_{skipped} = .5$, bootstrapped 95% CI [.07, .74]; Run 3: $r_{skipped} = .57$, bootstrapped 95% CI [.25, .79]; Run 4: $r_{skipped} = .36$, bootstrapped 95% CI [.02, .61]; Run 5: $r_{skipped} = .43$, bootstrapped 95% CI [.02, .66]; Run 6: $r_{skipped} = .39$, bootstrapped 95% CI [.03, .69]; Figure 5B). These results suggest that behaviorally relevant changes in functional connectivity occurred relatively early in training, providing a more granular view of the time course of learning than the before-and-after snapshots obtained from rest runs.

DISCUSSION

Repeated exposure to perceptual tasks improves behavioral performance. The current study examined the neural basis for such perceptual learning in the human brain. The specificity of perceptual learning suggests that it occurs at an early stage of visual processing, consistent with changes in early sensory areas observed with neurophysiology (Yan et al., 2014; Adab & Vogels, 2011; Raiguel et al., 2006; Yang & Maunsell, 2004; Schoups et al., 2001) and neuroimaging (Jia et al., 2020; Jehee et al., 2012; Bao et al., 2010; Yotsumoto et al., 2008; Kourtzi et al., 2005; Furmanski et al., 2004; Schwartz et al., 2002; Ress et al., 2000). The mechanism driving these changes is often assumed to be steepening (i.e., amplification or sharpening) of neuronal tuning curves in early sensory areas (e.g., Schwabe & Obermayer, 2005; Teich & Qian, 2003). Here, we tested an alternative mechanism whereby the connectivity between visual areas comes to more closely match the stimulus profile, improving the transmission of task-relevant information (Bejjanki et al., 2011).

Our findings provide evidence consistent with this matched filter hypothesis. After substantial exposure to a shape contour in one visual quadrant, there was robust and specific improvement in behavioral sensitivity to that trained shape relative to a mirrored control shape in the opposite quadrant. This was accompanied by an increase in resting functional connectivity between V1 and V4 voxels whose pRFs overlap the trained shape contour in retinotopic space. Furthermore, this neural change predicted the behavioral improvement across participants. Finally, we demonstrated that the enhanced functional connectivity between V1 and V4 voxels coding for the trained shape (relative to those coding for the control shape) begins to take on behavioral significance, in terms of predicting eventual differences in posttraining performance, early in training. Our findings are admittedly subtle and do not refute other accounts of perceptual learning in the brain; indeed, they may be compatible with the existence of multiple mechanisms. However, they do provide positive evidence for learning-induced plasticity in the connectivity between visual areas. Future studies will be needed to replicate and extend these findings with more statistical power, additional control groups, and/or different stimuli and tasks.

The current study may also provide a new perspective on past findings. For instance, Jehee et al. (2012) found that extensive practice on an orientation discrimination task resulted in selective enhancement of the neural representation of trained orientations in primary visual cortex. The authors speculated that their results might reflect a sharpening of the underlying population response, a reduction in noise correlations, or some combination. Our findings suggest that this could have been mediated by enhanced functional connectivity between the LGN and V1. As another example, Lewis et al. (2009) showed that perceptual learning can modulate resting connectivity in broad functional networks across the human brain in a task-specific manner. Our findings build upon this work by showing that perceptual learning can modulate fine-grained, retinotopically specific functional connectivity between early sensory areas to better match the stimulus profile.

Downloaded from direct.mit.edu/jocn/article-pdf/38/9/1695/2600227/jocn.a.2620.pdf by Yale University user on 13 October 2026

Future work could explore the extent to which the specific parameters of our study influenced the results. For instance, our results leave open the question as to how specific the observed effects are to the shapes we examined, given that we did not have a control condition with novel shapes in the trained location. Similarly, it is unclear whether the enhanced detection performance we also observe for the control shape in the posttest, which we attribute to a generic practice effect, is specific to the control shape or indicates some degree of generalization from the trained shape/quadrant. Furthermore, we utilized a task that has been shown to engender neural changes in early sensory areas (Kourtzi et al., 2005; Kourtzi, Tolias, Altmann, Augath, & Logothetis, 2003). Whether perceptual learning involves early or late areas (or both) is likely to depend on the difficulty of the task, the sensory modalities involved, and the nature of feedback and training received by participants (Diaz, Queirazza, & Philiastides, 2017; Kahnt, Grueschow, Speck, & Haynes, 2011; Chowdhury & DeAngelis, 2008; Law & Gold, 2008). For example, Kourtzi et al. (2005) failed to observe changes in early sensory areas when shape contours were presented in a "high-salience" configuration (background Gabors were uniformly oriented such that the target shape popped out); instead, changes occurred in later areas such as object-selective lateral occipital cortex.

Ultimately, the theoretical perspective that inspired our study (Bejjanki et al., 2011) could apply to perceptual learning in both earlier and later stages of processing, with changes in the synaptic strengths of connections between the corresponding brain regions improving the transmission of task-relevant information to subsequent stages. Indeed, Jia et al. (2020) used ultra-high-field laminar fMRI to show that extensive training on visual orientation discrimination leads to enhanced orientation-specific representations in primary visual cortex, as well as enhanced feedforward connectivity between early sensory areas and subsequent task-relevant decision areas. The authors concluded that this pattern is consistent with task-relevant reweighting of feedforward connectivity, providing further support for the matched filter hypothesis. In the current study, while our design does not allow us to directly ascertain the manner in which the transmission of task-relevant information is enhanced, similar reweighting of the synaptic strengths between areas V1 and V4 may be involved. We were also unable to ascertain whether the training, and concomitant connectivity changes, also produced changes (e.g., amplification or sharpening) at the level of neural tuning curves. Future work with a different design would be needed to relate the observed changes in connectivity to changes in tuning curves.

A notable feature of our study is that it involved only 1 hr (924 trials) of training within a single experimental session. Previous studies have documented neural and behavioral changes after a wide range of training durations, from single-shot to several days (Fine & Jacobs, 2002; Ahissar & Hochstein, 1997). Notably, although many studies have documented increased BOLD activation in early sensory areas as a result of perceptual learning, this effect appears to vanish after extensive practice, despite the persistence of behavioral improvements (Yotsumoto et al., 2008) and enhanced neural representations of task-relevant information (Jehee et al., 2012). Future work could examine the influence of more extended practice on task-relevant changes in resting functional connectivity (see Kang et al., 2018). On a related note, our results do not speak to the durability of changes in resting connectivity beyond the conclusion of the study. A future study could explore these changes over time and how their durability relates to the duration of training. Finally, an important consideration is that our experimental design did not allow us to definitively establish the extent to which enhanced engagement of top–down attention might have influenced our findings. The progressive improvement in behavioral performance we observe across training runs, together with enhanced posttraining performance specifically for the trained shape and the retinotopically specific changes in connectivity that are predictive of posttraining behavioral improvements, seem most parsimoniously interpreted as being due to task-specific learning. However, future studies will be needed to disentangle the influence of learning versus attention (e.g., by including a central cover task that engages top–down attention, while participants carry out perceptual learning in the periphery).

In conclusion, human observers have a remarkable capacity to selectively adapt their perceptual behavior in response to task demands. Here, we provide evidence that such perceptual learning is mediated, at least in part, by changes in network dynamics in the human brain that could enhance the fidelity with which task-relevant information is transmitted across cortical hierarchies.

Acknowledgments

We are grateful to M. Arcaro for assistance with retinotopic mapping.

Corresponding author: Vikranth Rao Bejjanki, 3058 Taylor Science Center, Hamilton College, Clinton, NY 13323, e-mail: bejjanki@hamilton.edu.

Data Availability Statement

Researchers may access the study data via e-mail to the lead author (bejjanki@hamilton.edu).

Funding Information

This work was supported by NIH R01 EY021755 and the Canadian Institute for Advanced Research.

Diversity in Citation Practices

Retrospective analysis of the citations in every article published in this journal from 2010 to 2021 reveals a persistent

Downloaded from direct.mit.edu/jocn/article-pdf/38/9/1695/2600227/jocn.a.2620.pdf by Yale University user on 13 October 2026

pattern of gender imbalance: Although the proportions of authorship teams (categorized by estimated gender identification of first author/last author) publishing in the *Journal of Cognitive Neuroscience* (*JoCN*) during this period were M(an)/M = .407, W(oman)/M = .32, M/W = .115, and W/W = .159, the comparable proportions for the articles that these authorship teams cited were M/M = .549, W/M = .257, M/W = .109, and W/W = .085 (Postle and Fulvio, *JoCN*, 34:1, pp. 1–3). Consequently, *JoCN* encourages all authors to consider gender balance explicitly when selecting which articles to cite and gives them the opportunity to report their article's gender citation balance. The authors of this paper report its proportions of citations by gender category to be: M/M = .61; W/M = .186; M/W = .119; W/W = .085.

REFERENCES

Adab, H. Z., & Vogels, R. (2011). Practicing coarse orientation discrimination improves orientation signals in macaque cortical area V4. *Current Biology*, *21*, 1661–1666. https://doi.org/10.1016/j.cub.2011.08.037, PubMed: 21962714

Ahissar, M., & Hochstein, S. (1997). Task difficulty and the specificity of perceptual learning. *Nature*, *387*, 401–406. https://doi.org/10.1038/387401a0, PubMed: 9163425

Al-Aidroos, N., Said, C. P., & Turk-Browne, N. B. (2012). Top–down attention switches coupling between low-level and high-level areas of human visual cortex. *Proceedings of the National Academy of Sciences, U.S.A.*, *109*, 14675–14680. https://doi.org/10.1073/pnas.1202095109, PubMed: 22908274

Aly, M., & Turk-Browne, N. B. (2016). Attention stabilizes representations in the human hippocampus. *Cerebral Cortex*, *26*, 783–796. https://doi.org/10.1093/cercor/bhv041, PubMed: 25766839

Arcaro, M. J., McMains, S. A., Singer, B. D., & Kastner, S. (2009). Retinotopic organization of human ventral visual cortex. *Journal of Neuroscience*, *29*, 10638–10652. https://doi.org/10.1523/jneurosci.2807-09.2009, PubMed: 19710316

Averbeck, B. B., Latham, P. E., & Pouget, A. (2006). Neural correlations, population coding and computation. *Nature Review Neuroscience*, *7*, 358–366. https://doi.org/10.1038/nrn1888, PubMed: 16760916

Bao, M., Yang, L., Rios, C., He, B., & Engel, S. A. (2010). Perceptual learning increases the strength of the earliest signals in visual cortex. *Journal of Neuroscience*, *30*, 15080–15084. https://doi.org/10.1523/JNEUROSCI.5703-09.2010, PubMed: 21068313

Bejjanki, V. R., Beck, J. M., Lu, Z.-L., & Pouget, A. (2011). Perceptual learning as improved probabilistic inference in early sensory areas. *Nature Neuroscience*, *14*, 642–648. https://doi.org/10.1038/nn.2796, PubMed: 21460833

Biswal, B., Yetkin, F. Z., Haughton, V. M., & Hyde, J. S. (1995). Functional connectivity in the motor cortex of resting human brain using echo-planar MRI. *Magnetic Resonance in Medicine*, *34*, 537–541. https://doi.org/10.1002/mrm.1910340409, PubMed: 8524021

Chowdhury, S. A., & DeAngelis, G. C. (2008). Fine discrimination training alters the causal contribution of macaque area MT to depth perception. *Neuron*, *60*, 367–377. https://doi.org/10.1016/j.neuron.2008.08.023, PubMed: 18957227

Cox, R. W. (1996). AFNI: Software for analysis and visualization of functional magnetic resonance neuroimages. *Computers and Biomedical Research*, *29*, 162–173. https://doi.org/10.1006/cbmr.1996.0014, PubMed: 8812068

Crist, R. E., Kapadia, M. K., Westheimer, G., & Gilbert, C. D. (1997). Perceptual learning of spatial localization: Specificity for orientation, position, and context. *Journal of Neurophysiology*, *78*, 2889–2894. https://doi.org/10.1152/jn.1997.78.6.2889, PubMed: 9405509

Dale, A. M., Fischl, B., & Sereno, M. I. (1999). Cortical surface-based analysis: I. Segmentation and surface reconstruction. *Neuroimage*, *9*, 179–194. https://doi.org/10.1006/nimg.1998.0395, PubMed: 9931268

Diaz, J. A., Queirazza, F., & Philiastides, M. G. (2017). Perceptual learning alters post-sensory processing in human decision-making. *Nature Human Behaviour*, *1*, 0035. https://doi.org/10.1038/s41562-016-0035

Donaldson, W. (1992). Measuring recognition memory. *Journal of Experimental Psychology: General*, *121*, 275–277. https://doi.org/10.1037/0096-3445.121.3.275, PubMed: 1402701

Dumoulin, S. O., & Wandell, B. A. (2008). Population receptive field estimates in human visual cortex. *Neuroimage*, *39*, 647–660. https://doi.org/10.1016/j.neuroimage.2007.09.034, PubMed: 17977024

Efron, B., & Tibshirani, R. (1986). Bootstrap methods for standard errors, confidence intervals, and other measures of statistical accuracy. *Statistical Science*, *1*, 54–75. https://doi.org/10.1214/ss/1177013815

Engel, S. A., Glover, G. H., & Wandell, B. A. (1997). Retinotopic organization in human visual cortex and the spatial precision of functional MRI. *Cerebral Cortex*, *7*, 181–192. https://doi.org/10.1093/cercor/7.2.181, PubMed: 9087826

Fahle, M., Edelman, S., & Poggio, T. (1995). Fast perceptual learning in hyperacuity. *Vision Research*, *35*, 3003–3013. https://doi.org/10.1016/0042-6989(95)00044-Z, PubMed: 8533337

Fahle, M., & Morgan, M. (1996). No transfer of perceptual learning between similar stimuli in the same retinal position. *Current Biology*, *6*, 292–297. https://doi.org/10.1016/S0960-9822(02)00479-7, PubMed: 8805246

Ferster, D., & Miller, K. D. (2000). Neural mechanisms of orientation selectivity in the visual cortex. *Annual Reviews in Neuroscience*, *23*, 441–471. https://doi.org/10.1146/annurev.neuro.23.1.441, PubMed: 10845071

Fine, I., & Jacobs, R. A. (2002). Comparing perceptual learning tasks: A review. *Journal of Vision*, *2*, 190–203. https://doi.org/10.1167/2.2.5, PubMed: 12678592

Fiorentini, A., & Berardi, N. (1980). Perceptual learning specific for orientation and spatial frequency. *Nature*, *287*, 43–44. https://doi.org/10.1038/287043a0, PubMed: 7412873

Fisher, A. V., & Sloutsky, V. M. (2005). When induction meets memory: Evidence for gradual transition from similarity-based to category-based induction. *Child Development*, *76*, 583–597. https://doi.org/10.1111/j.1467-8624.2005.00865.x, PubMed: 15892780

Fox, M. D., & Raichle, M. E. (2007). Spontaneous fluctuations in brain activity observed with functional magnetic resonance imaging. *Nature Reviews Neuroscience*, *8*, 700–711. https://doi.org/10.1038/nrn2201, PubMed: 17704812

Fox, M. D., Snyder, A. Z., Zacks, J. M., & Raichle, M. E. (2006). Coherent spontaneous activity accounts for trial-to-trial variability in human evoked brain responses. *Nature Neuroscience*, *9*, 23–25. https://doi.org/10.1038/nn1616, PubMed: 16341210

Furmanski, C. S., Schluppeck, D., & Engel, S. A. (2004). Learning strengthens the response of primary visual cortex to simple patterns. *Current Biology*, *14*, 573–578. https://doi.org/10.1016/j.cub.2004.03.032, PubMed: 15062097

Downloaded from direct.mit.edu/jocn/article-pdf/38/9/1695/2600227/jocn.a.2620.pdf by Yale University user on 13 October 2026

Gibson, E. J. (1963). Perceptual learning. *Annual Review of Psychology*, *14*, 29–56. https://doi.org/10.1146/annurev.ps.14.020163.000333, PubMed: 13947716

Gilbert, C. D., Sigman, M., & Crist, R. E. (2001). The neural basis of perceptual learning. *Neuron*, *31*, 681–697. https://doi.org/10.1016/S0896-6273(01)00424-X, PubMed: 11567610

Griffis, J. C., Elkhetali, A. S., Burge, W. K., Chen, R. H., & Visscher, K. M. (2015). Retinotopic patterns of background connectivity between V1 and fronto-parietal cortex are modulated by task demands. *Frontiers in Human Neuroscience*, *9*, 338. https://doi.org/10.3389/fnhum.2015.00338, PubMed: 26106320

Harvey, B. M., & Dumoulin, S. O. (2011). The relationship between cortical magnification factor and population receptive field size in human visual cortex: Constancies in cortical architecture. *Journal of Neuroscience*, *31*, 13604–13612. https://doi.org/10.1523/JNEUROSCI.2572-11.2011, PubMed: 21940451

Hubel, D. H., & Wiesel, T. N. (1968). Receptive fields and functional architecture of monkey striate cortex. *Journal of Physiology*, *195*, 215–243. https://doi.org/10.1113/jphysiol.1968.sp008455, PubMed: 4966457

Jehee, J. F. M., Ling, S., Swisher, J. D., van Bergen, R. S., & Tong, F. (2012). Perceptual learning selectively refines orientation representations in early visual cortex. *Journal of Neuroscience*, *32*, 16747–16753. https://doi.org/10.1523/JNEUROSCI.6112-11.2012, PubMed: 23175828

Jia, K., Zamboni, E., Kemper, V., Rua, C., Goncalves, N. R., Ng, A. K. T., et al. (2020). Recurrent processing drives perceptual plasticity. *Current Biology*, *30*, 4177–4187. https://doi.org/10.1016/j.cub.2020.08.016, PubMed: 32888488

Kahnt, T., Grueschow, M., Speck, O., & Haynes, J.-D. (2011). Perceptual learning and decision-making in human medial frontal cortex. *Neuron*, *70*, 549–559. https://doi.org/10.1016/j.neuron.2011.02.054, PubMed: 21555079

Kang, D.-W., Kim, D., Chang, L.-H., Kim, Y.-H., Takahashi, E., Cain, M. S., et al. (2018). Structural and functional connectivity changes beyond visual cortex in a later phase of visual perceptual learning. *Scientific Reports*, *8*, 5186. https://doi.org/10.1038/s41598-018-23487-z, PubMed: 29581455

Karni, A., & Sagi, D. (1991). Where practice makes perfect in texture discrimination: Evidence for primary visual cortex plasticity. *Proceedings of the National Academy of Sciences, U.S.A.*, *88*, 4966–4970. https://doi.org/10.1073/pnas.88.11.4966, PubMed: 2052578

Kastner, S., De Weerd, P., & Ungerleider, L. G. (2000). Texture segregation in the human visual cortex: A functional MRI study. *Journal of Neurophysiology*, *83*, 2453–2457. https://doi.org/10.1152/jn.2000.83.4.2453, PubMed: 10758146

Kohn, A., Coen-Cagli, R., Kanitscheider, I., & Pouget, A. (2016). Correlations and neuronal population information. *Annual Review Neuroscience*, *39*, 237–256. https://doi.org/10.1146/annurev-neuro-070815-013851, PubMed: 27145916

Kourtzi, Z., Betts, L. R., Sarkheil, P., & Welchman, A. E. (2005). Distributed neural plasticity for shape learning in the human visual cortex. *PLoS Biology*, *3*, e204. https://doi.org/10.1371/journal.pbio.0030204, PubMed: 15934786

Kourtzi, Z., Tolias, A. S., Altmann, C. F., Augath, M., & Logothetis, N. K. (2003). Integration of local features into global shapes: Monkey and human fMRI studies. *Neuron*, *37*, 333–346. https://doi.org/10.1016/s0896-6273(02)01174-1, PubMed: 12546827

Law, C.-T., & Gold, J. I. (2008). Neural correlates of perceptual learning in a sensory-motor, but not a sensory, cortical area. *Nature Neuroscience*, *11*, 505–513. https://doi.org/10.1038/nn2070, PubMed: 18327253

Lee, I. A., & Preacher, K. J. (2013). *Calculation for the test of the difference between two dependent correlations with no variable in common* [Computer software]. Available from https://quantpsy.org.

Lewis, C. M., Baldassarre, A., Committeri, G., Romani, G. L., & Corbetta, M. (2009). Learning sculpts the spontaneous activity of the resting human brain. *Proceedings of the National Academy of Sciences, U.S.A.*, *106*, 17558–17563. https://doi.org/10.1073/pnas.0902455106, PubMed: 19805061

Lu, Z.-L., & Dosher, B. A. (2022). Current directions in visual perceptual learning. *Nature Reviews Psychology*, *1*, 654–668. https://doi.org/10.1038/s44159-022-00107-2, PubMed: 37274562

Nauhaus, I., Nielsen, K. J., Disney, A. A., & Callaway, E. M. (2012). Orthogonal micro-organization of orientation and spatial frequency in primate primary visual cortex. *Nature Neuroscience*, *15*, 1683–1690. https://doi.org/10.1038/nn.3255, PubMed: 23143516

Ni, A. M., Ruff, D. A., Alberts, J. J., Symmonds, J., & Cohen, M. R. (2018). Learning and attention reveal a general relationship between population activity and behavior. *Science*, *359*, 463–465. https://doi.org/10.1126/science.aao0284, PubMed: 29371470

Norman-Haignere, S. V., McCarthy, G., Chun, M. M., & Turk-Browne, N. B. (2012). Category-selective background connectivity in ventral visual cortex. *Cerebral Cortex*, *22*, 391–402. https://doi.org/10.1093/cercor/bhr118, PubMed: 21670097

Pernet, C. R., Wilcox, R., & Rousselet, G. A. (2013). Robust correlation analyses: False positive and power validation using a new open source matlab toolbox. *Frontiers in Psychology*, *3*, 606. https://doi.org/10.3389/fpsyg.2012.00606, PubMed: 23335907

Raiguel, S., Vogels, R., Mysore, S. G., & Orban, G. A. (2006). Learning to see the difference specifically alters the most informative V4 neurons. *Journal of Neuroscience*, *26*, 6589–6602. https://doi.org/10.1523/JNEUROSCI.0457-06.2006, PubMed: 16775147

Recanzone, G. H., Jenkins, W. M., Hradek, G. T., & Merzenich, M. M. (1992). Progressive improvement in discriminative abilities in adult owl monkeys performing a tactile frequency discrimination task. *Journal of Neurophysiology*, *67*, 1015–1030. https://doi.org/10.1152/jn.1992.67.5.1015, PubMed: 1597695

Recanzone, G. H., Schreiner, C. E., & Merzenich, M. M. (1993). Plasticity in the frequency representation of primary auditory cortex following discrimination training in adult owl monkeys. *Journal of Neuroscience*, *13*, 87–103. https://doi.org/10.1523/JNEUROSCI.13-01-00087.1993, PubMed: 8423485

Reppa, I., Williams, K. E., Greville, W. J., & Saunders, J. (2020). The relative contribution of shape and colour to object memory. *Memory & Cognition*, *48*, 1504–1521. https://doi.org/10.3758/s13421-020-01058-w, PubMed: 32542477

Ress, D., Backus, B. T., & Heeger, D. J. (2000). Activity in primary visual cortex predicts performance in a visual detection task. *Nature Neuroscience*, *3*, 940–945. https://doi.org/10.1038/78856, PubMed: 10966626

Riesenhuber, M., & Poggio, T. (2000). Models of object recognition. *Nature Neuroscience*, *3*, 1199–1204. https://doi.org/10.1038/81479, PubMed: 11127838

Schoups, A., Vogels, R., Qian, N., & Orban, G. (2001). Practising orientation identification improves orientation coding in V1 neurons. *Nature*, *412*, 549–553. https://doi.org/10.1038/35087601, PubMed: 11484056

Schwabe, L., & Obermayer, K. (2005). Adaptivity of tuning functions in a generic recurrent network model of a cortical hypercolumn. *Journal of Neuroscience*, *25*, 3323–3332.

Downloaded from direct.mit.edu/jocn/article-pdf/38/9/1695/2600227/jocn.a.2620.pdf by Yale University user on 13 October 2026

https://doi.org/10.1523/JNEUROSCI.4493-04.2005, PubMed: 15800187
Schwartz, S., Maquet, P., & Frith, C. (2002). Neural correlates of perceptual learning: A functional MRI study of visual texture discrimination. *Proceedings of the National Academy of Sciences, U.S.A.*, *99*, 17137–17142. https://doi.org/10.1073/pnas.242414599, PubMed: 12446842
Seitz, A., & Watanabe, T. (2005). A unified model for perceptual learning. *Trends in Cognitive Science*, *9*, 329–334. https://doi.org/10.1016/j.tics.2005.05.010, PubMed: 15955722
Seriès, P., Latham, P. E., & Pouget, A. (2004). Tuning curve sharpening for orientation selectivity: Coding efficiency and the impact of correlations. *Nature Neuroscience*, *7*, 1129–1135. https://doi.org/10.1038/nn1321, PubMed: 15452579
Simmons, W. K., Bellgowan, P. S. F., & Martin, A. (2007). Measuring selectivity in fMRI data. *Nature Neuroscience*, *10*, 4–5. https://doi.org/10.1038/nn0107-4, PubMed: 17189941
Smith, S. M., Jenkinson, M., Woolrich, M. W., Beckmann, C. F., Behrens, T. E. J., Johansen-Berg, H., et al. (2004). Advances in functional and structural MR image analysis and implementation as FSL. *Neuroimage*, *23(Suppl. 1)*, S208–S219. https://doi.org/10.1016/j.neuroimage.2004.07.051, PubMed: 15501092
Smith, M. A., & Kohn, A. (2008). Spatial and temporal scales of neuronal correlation in primary visual cortex. *Journal of Neuroscience*, *28*, 12591–12603. https://doi.org/10.1523/jneurosci.2929-08.2008, PubMed: 19036953
Snodgrass, J. G., & Corwin, J. (1988). Pragmatics of measuring recognition memory: Applications to dementia and amnesia. *Journal of Experimental Psychology: General*, *117*, 34–50. https://doi.org/10.1037/0096-3445.117.1.34, PubMed: 2966230
Spiridon, M., & Gerstner, W. (2001). Effect of lateral connections on the accuracy of the population code for a network of spiking neurons. *Network*, *12*, 409–421. https://doi.org/10.1080/net.12.4.409.421, PubMed: 11762897
Steiger, J. H. (1980). Tests for comparing elements of a correlation matrix. *Psychological Bulletin*, *87*, 245–251. https://doi.org/10.1037/0033-2909.87.2.245
Teich, A. F., & Qian, N. (2003). Learning and adaptation in a recurrent model of V1 orientation selectivity. *Journal of Neurophysiology*, *89*, 2086–2100. https://doi.org/10.1152/jn.00970.2002, PubMed: 12611961
Thielscher, A., Kölle, M., Neumann, H., Spitzer, M., & Grön, G. (2008). Texture segmentation in human perception: A combined modeling and fMRI study. *Neuroscience*, *151*, 730–736. https://doi.org/10.1016/j.neuroscience.2007.11.040, PubMed: 18191901
Tompary, A., Al-Aidroos, N., & Turk-Browne, N. B. (2018). Attending to what and where: Background connectivity integrates categorical and spatial attention. *Journal of Cognitive Neuroscience*, *30*, 1281–1297. https://doi.org/10.1162/jocn_a_01284, PubMed: 29791296
Wallis, G., & Rolls, E. T. (1997). Invariant face and object recognition in the visual system. *Progress in Neurobiology*, *51*, 167–194. https://doi.org/10.1016/S0301-0082(96)00054-8, PubMed: 9247963
Wandell, B. A., Dumoulin, S. O., & Brewer, A. A. (2007). Visual field maps in human cortex. *Neuron*, *56*, 366–383. https://doi.org/10.1016/j.neuron.2007.10.012, PubMed: 17964252
Watanabe, T., Náñez, J. E., Sr., Koyama, S., Mukai, I., Liederman, J., & Sasaki, Y. (2002). Greater plasticity in lower-level than higher-level visual motion processing in a passive perceptual learning task. *Nature Neuroscience*, *5*, 1003–1009. https://doi.org/10.1038/nn915, PubMed: 12219093
Yan, Y., Rasch, M. J., Chen, M., Xiang, X., Huang, M., Wu, S., et al. (2014). Perceptual training continuously refines neuronal population codes in primary visual cortex. *Nature Neuroscience*, *17*, 1380–1387. https://doi.org/10.1038/nn.3805, PubMed: 25195103
Yang, T., & Maunsell, J. H. R. (2004). The effect of perceptual learning on neuronal responses in monkey visual area V4. *Journal of Neuroscience*, *24*, 1617–1626. https://doi.org/10.1523/JNEUROSCI.4442-03.2004, PubMed: 14973244
Yotsumoto, Y., Watanabe, T., & Sasaki, Y. (2008). Different dynamics of performance and brain activation in the time course of perceptual learning. *Neuron*, *57*, 827–833. https://doi.org/10.1016/j.neuron.2008.02.034, PubMed: 18367084
Zohary, E., Shadlen, M. N., & Newsome, W. T. (1994). Correlated neuronal discharge rate and its implications for psychophysical performance. *Nature*, *370*, 140–143. https://doi.org/10.1038/370140a0, PubMed: 8022482

Downloaded from direct.mit.edu/jocn/article-pdf/38/9/1695/2600227/jocn.a.2620.pdf by Yale University user on 13 October 2026